Search for anomalous quartic gauge couplings in the process $\mu^+\mu^- \to \bar{\nu}\nu\gamma\gamma$ with a nested local outlier factor

Ke-Xin Chen, Yu-Chen Guo and Ji-Chong Yang⋆

Department of Physics, Liaoning Normal University,
No. 850 Huanghe Road, Dalian 116029, China
Center for Theoretical and Experimental High Energy Physics, Liaoning Normal University,
No. 850 Huanghe Road, Dalian 116029, China

⋆ yangjichong@lnnu.edu.cn

Abstract

In recent years, with the increasing luminosities of colliders, handling the growing amount of data has become a major challenge for future new physics (NP) phenomenological research. To improve efficiency, machine learning algorithms have been introduced into the field of high-energy physics. As a machine learning algorithm, the local outlier factor (LOF), and the nested LOF (NLOF) are potential tools for NP phenomenological studies. In this work, the possibility of searching for the signals of anomalous quartic gauge couplings (aQGCs) at muon colliders using the NLOF is investigated. Taking the process $\mu^+\mu^- \to \nu\bar{\nu}\gamma\gamma$ as an example, the signals of dimension-8 aQGCs are studied, expected coefficient constraints are presented. The event selection strategy uses unsupervised anomaly scores, with supervised optimization for EFT sensitivity. The NLOF algorithm is shown to outperform the k-means based anomaly detection methods, and a traditional counterpart.

1 Introduction

As the Large Hadron Collider (LHC) experiment transitions into the post-Higgs discovery phase, physicists have embarked on the quest for new physics (NP) beyond the Standard Model (SM) [1, 2], which is widely believed to exist at higher energy scales. The pursuit of NP has emerged as a leading frontier in high energy physics (HEP) research. HEP investigations frequently entail the analysis of extensive datasets stemming from particle collisions or other experimental endeavors. Given the fact that, in the foreseeable next decade or so, upgrades of colliders will focus primarily on luminosity rather than energy, the efficiency of data analyzing becomes a more and more important topic.

Machine learning (ML) promises to substantially speed up data processing and analysis, thereby serving as a pivotal tool in advancing the detection of NP signals. To efficiently analyze data within this context, previous studies have applied anomaly detection (AD) ML algorithms in the field of HEP for the purpose of searching for NP signals. [3–25]. In AD algorithms, one notable method is the local outlier factor (LOF) [26]. As a density-based AD algorithm, it can be expected to effectively screen signals of NP when combined with the nested anomaly detection algorithm [27], even when interference terms play a significant role. Compared to the nested isolation forest method used in Refs. [27], an additional motivation for our investigation of LOF's effectiveness lies in that, the core computation in LOF primarily involves calculating point-to-point distances. Even when extended with nesting, as in the nested LOF (NLOF) algorithm proposed in this study, the computational backbone remains anchored in distance calculations. This grants both LOF and NLOF inherent flexibility, i.e., we can strategically define various kernel functions, precompute inter-point distances, and subsequently input them within (N)LOF frameworks. Notably, with the recent surge of quantum ML applications in NP searches, quantum computing as a high-throughput data processing paradigm, enables ultra-efficient distance computation through quantum kernels. This naturally facilitates quantum-enhanced extensions, quantum kernel (N)LOF in the future. As an unsupervised ML algorithm, the LOF can automatically discover the anomalies, which is even useful if there was no NP signals, because it can be expected that the signal of rare processes or the possible artifacts of the colliders can emerge as anomalous signals. When NLOF is introduced, although the algorithm needs a reference dataset from the SM, it does not need information about the NP models, i.e., it can search for NP without knowing what NP model it is searching for. It is worth noting that, in practical implementation, to highlight the signal for a certain NP model, supervised optimization specific for this NP model can be introduced.

As a validation, we consider the Standard Model Effective Field Theory (SMEFT) [28–33]. The prominence of SMEFT stems precisely from its applicability in high-luminosity regimes where collision energies remain below the threshold required to directly excite NP degrees of freedom, making it inherently aligned with this study's focus. Concurrently, the muon collider is considered as the experimental scenario [34–42]. As a lepton collider, it offers high luminosity and relatively clean QCD backgrounds. It is worth noting that, as a geometrically well-defined algorithm, the (N)LOF algorithms are fundamentally agnostic to the specific NP models under investigation, and should remain universally applicable across arbitrary collider configurations and theoretical frameworks.

The muon collider is recognized as an effective gauge boson collider, particularly suited for probing vector boson scattering (VBS) processes. Among these, the $WW \to \gamma\gamma$ channel stands out as a prominent VBS candidate due to its distinct advantages, including absence of forward-moving charged leptons, and no additional electroweak (EW) vertices. As a consequence, this study focuses on the process $\mu^+\mu^- \to \nu\bar{\nu}\gamma\gamma$. As a VBS process, the process $\mu^+\mu^- \to \nu\bar{\nu}\gamma\gamma$ is suitable to study the SMEFT operators contributing to anomalous quartic gauge couplings (aQGCs) [43–47]. High dimensional operators generating aQGCs independent of anomalous triple gauge couplings emerge starting at dimension-8 in the SMEFT. Therefore the signals of dimension-8 aQGCs operators in the $\mu^+\mu^- \to \nu\bar{\nu}\gamma\gamma$ is adopted in this work, which thus serves as a timely complement to the growing interest in dimension-8 operator analyses [48–58], and directly align with the current focus in NP phenomenology that prioritizes precision EW measurements and high-dimensional operator disentanglement at future colliders.

It is worth clarifying that if the goal were solely to identify anomalous events, one would not need to know the NP model. However, if no trace of NP were found, the purpose of NP phenomenology becomes constraining the parameters of NP. To achieve this, introducing an NP model becomes necessary. In our phenomenological study, not only the aQGCs are introduced, but also an event selection strategy designed to maximize the signal is adopted, which incorporates supervised learning. To investigate the impact of developing event selection criteria using only background events, the scenarios are also considered where the number of remaining background events is 1%, 5%, and 10%.

The remainder of the paper is organized as follows. In section 2, a brief introduction to aQGCs and the $\mu^+\mu^- \to \nu\bar{\nu}\gamma\gamma$ process is given. The event selection strategy of (N)LOF is discussed in section 3. Section 4 presents numerical results for the expected coefficient constraints. Section 5 is a summary of the conclusions.
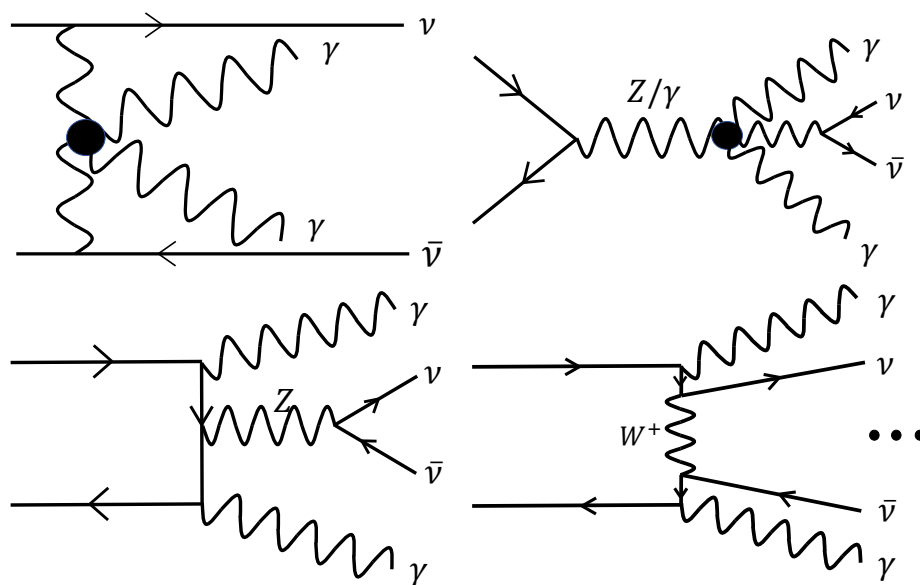
Figure 1: Typical Feynman diagrams for signal events (the upper panels) and background events (the lower panels).

2 aQGCs and the process $\mu^+\mu^- \to \nu\bar{\nu}\gamma\gamma$ at the muon colliders

A key concern in NP phenomenological studies is the sensitivity of processes at (future) colliders to NP models. To form a cross-reference with other studies [59–74], we use the most commonly used set of dimension-8 aQGCs operators [75,76]. Only the operators mixed transverse and longitudinal operators O_{M_i} and the transverse operators O_{T_i} in this operator set are involved in the process $\mu^+\mu^- \to \nu\bar{\nu}\gamma\gamma$, the Lagrangian is,

$$\mathcal{L}_{\text{aQGC}} = \sum_i \frac{f_{M_i}}{\Lambda^4} O_{M_i} + \sum_j \frac{f_{T_j}}{\Lambda^4} O_{T_j}, \tag{1}$$

where f_{M_i} and f_{T_j} are dimensionless Wilson coefficients, and Λ is the NP energy scale. The operators $O_{M_{0,1,2,3,4,5,7}}$ and $O_{T_{0,1,2,5,6,7}}$ can contribute to the process of $\mu^+\mu^- \to \nu\bar{\nu}\gamma\gamma$ at muon colliders,

$$\begin{aligned}
O_{M_0} &= \text{Tr}\left[\widehat{W}_{\mu\nu}\widehat{W}^{\mu\nu}\right] \times \left[\left(D^\beta\Phi\right)^\dagger D^\beta\Phi\right], \\
O_{M_1} &= \text{Tr}\left[\widehat{W}_{\mu\nu}\widehat{W}^{\nu\beta}\right] \times \left[\left(D^\beta\Phi\right)^\dagger D^\mu\Phi\right], \\
O_{M_2} &= \left[B_{\mu\nu}B^{\mu\nu}\right] \times \left[(D_\beta\Phi)^\dagger D^\beta\Phi\right], \\
O_{M_3} &= \left[B_{\mu\nu}B^{\nu\beta}\right] \times \left[(D_\beta\Phi)^\dagger D^\mu\Phi\right], \\
O_{M_4} &= \left[(D_\mu\Phi)^\dagger\widehat{W}_{\alpha\nu}D^\mu\Phi\right] \times B^{\beta\nu}, \\
O_{M_5} &= \left[\left(D_\mu\Phi\right)^\dagger\widehat{W}_{\beta\nu}D_\nu\Phi\right] \times B^{\beta\mu} + h.c., \\
O_{M_7} &= \left(D_\mu\Phi\right)^\dagger\widehat{W}_{\beta\nu}\widehat{W}_{\beta\mu}D_\nu\Phi, \\
O_{T_0} &= \text{Tr}\left[\widehat{W}_{\mu\nu}\widehat{W}^{\mu\nu}\right] \times \text{Tr}\left[\widehat{W}_{\alpha\beta}\widehat{W}^{\alpha\beta}\right], \\
O_{T_1} &= \text{Tr}\left[\widehat{W}_{\alpha\nu}\widehat{W}^{\mu\beta}\right] \times \text{Tr}\left[\widehat{W}_{\mu\beta}\widehat{W}^{\alpha\nu}\right], \\
O_{T_2} &= \text{Tr}\left[\widehat{W}_{\alpha\mu}\widehat{W}^{\mu\beta}\right] \times \text{Tr}\left[\widehat{W}_{\beta\nu}\widehat{W}^{\nu\alpha}\right], \\
O_{T_5} &= \text{Tr}\left[\widehat{W}_{\mu\nu}\widehat{W}^{\mu\nu}\right] \times B_{\alpha\beta}B^{\alpha\beta}, \\
O_{T_6} &= \text{Tr}\left[\widehat{W}_{\alpha\nu}\widehat{W}^{\mu\beta}\right] \times B_{\mu\beta}B^{\alpha\nu}, \\
O_{T_7} &= \text{Tr}\left[\widehat{W}_{\alpha\mu}\widehat{W}^{\mu\beta}\right] \times B_{\beta\nu}B^{\nu\alpha},
\end{aligned} \tag{2}$$

where $\widehat{W} \equiv \vec{\sigma}\cdot\vec{W}/2$ with σ being the Pauli matrices and $\vec{W} = \{W^1, W^2, W^3\}$, B_μ and W_μ^i stand for the gauge fields of $U(1)_Y$ and $SU(2)_I$, $B_{\mu\nu}$ and $W_{\mu\nu}$ are field strength tensors, and $D_\mu\Phi$ is the covariant derivative. The typical Feynman diagrams are shown in Fig. 1. The absence of forward-moving charged leptons in the final state, as well as the fact that the final state of the VBS subprocess is two photons which avoids the introduction of additional EW vertices, makes it well suited for exploring the aQGCs. At the muon colliders, the VBS processes are associated with very energetic muons or neutrinos in the forward region with respect to the beam. One important background could be the beam induced background, especially those with the final states containing soft/collinear photons/muons which can escape from the detectors and mimic the neutrinos. It is challenging to generate events with soft/collinear final states using Monte Carlo (MC) methods, as they often lead to infrared divergences, making such backgrounds difficult to study, especially at the current stage when the detector has not yet been constructed. In this work, we neglect the contribution from these backgrounds.

As an effective field theory, the SMEFT is only valid under the NP energy scale. The high center-of-mass (c.m.) energy achievable at muon colliders offers an excellent opportunity to detect potential NP signals. However, it is necessary to verify the validity of the SMEFT framework. Partial wave unitarity has been extensively employed in previous studies as a criterion for assessing the validity of the SMEFT [77–85]. Partial-wave unitarity bounds are

Table 1: The tightest partial wave unitarity bounds at $\sqrt{s} = 3$ TeV and 10 TeV.

$\sqrt{s}$	3 TeV	10 TeV
$\left\lvert f_{M_0}/\Lambda^4 \right\rvert$ (TeV^{-4})	8.2	6.6×10^{-2}
$\left\lvert f_{M_1}/\Lambda^4 \right\rvert$ (TeV^{-4})	32.7	2.6×10^{-1}
$\left\lvert f_{M_2}/\Lambda^4 \right\rvert$ (TeV^{-4})	1.2	1.0×10^{-2}
$\left\lvert f_{M_3}/\Lambda^4 \right\rvert$ (TeV^{-4})	4.9	3.9×10^{-2}
$\left\lvert f_{M_4}/\Lambda^4 \right\rvert$ (TeV^{-4})	4.5	3.6×10^{-2}
$\left\lvert f_{M_5}/\Lambda^4 \right\rvert$ (TeV^{-4})	9.0	7.3×10^{-2}
$\left\lvert f_{M_7}/\Lambda^4 \right\rvert$ (TeV^{-4})	65.4	5.3×10^{-1}
$\left\lvert f_{T_0}/\Lambda^4 \right\rvert$ (TeV^{-4})	1.9	1.5×10^{-2}
$\left\lvert f_{T_1}/\Lambda^4 \right\rvert$ (TeV^{-4})	5.7	4.6×10^{-2}
$\left\lvert f_{T_2}/\Lambda^4 \right\rvert$ (TeV^{-4})	7.6	6.1×10^{-2}
$\left\lvert f_{T_5}/\Lambda^4 \right\rvert$ (TeV^{-4})	0.57	4.6×10^{-3}
$\left\lvert f_{T_6}/\Lambda^4 \right\rvert$ (TeV^{-4})	1.7	1.4×10^{-2}
$\left\lvert f_{T_7}/\Lambda^4 \right\rvert$ (TeV^{-4})	2.3	1.8×10^{-2}

process-specific. When using an EFT to study a process at a given energy scale, if the Wilson coefficients are sufficiently large such that the amplitude violates unitarity, it indicates that the EFT fails to provide a consistent description of the process under those coefficients and at that energy. For the subprocess $WW \rightarrow \gamma\gamma$, in the c.m. frame with z-axis along the flight direction of W^- in the initial state, the helicity amplitude can be expanded using the Wigner d-function as [77],

$$\mathcal{M}(W^-_{\lambda_1} W^+_{\lambda_2} \rightarrow \gamma_{\lambda_3} \gamma_{\lambda_4}) = 8\pi \sum_J (2J+1)\sqrt{1+\delta_{\lambda_3\lambda_4}} \, e^{i(\lambda-\lambda')\phi} d^J_{\lambda\lambda'}(\theta) T^J , \qquad (3)$$

where $\lambda_{1,2} = \pm 1, 0$ and $\lambda_{3,4} = \pm 1$ correspond to the helicities of the vector bosons, θ and ϕ are zenith and azimuth angles of γ_{λ_3}, $\lambda = \lambda_1 - \lambda_2$, $\lambda' = \lambda_3 - \lambda_4$, and T_J is the coefficient of the expansion. The partial wave unitarity bound is $|T^J| \leq 2$ [80]. The results of the helicity amplitudes as well as the $|T^J|$ are calculated in Ref. [24], the tightest bounds for each operator are obtained. For the subprocess $WW \rightarrow \gamma\gamma$, the results of the partial wave unitarity bounds for one operator at a time are [24]

$$\left\lvert \frac{f_{M_0}}{\Lambda^4} \right\rvert \leq \frac{128\sqrt{2}\pi M_W^2}{\hat{s}^2 e^2 v^2} , \qquad \left\lvert \frac{f_{M_1}}{\Lambda^4} \right\rvert \leq \frac{512\sqrt{2}\pi M_W^2}{\hat{s}^2 e^2 v^2} ,$$

$$\left\lvert \frac{f_{M_2}}{\Lambda^4} \right\rvert \leq \frac{64\sqrt{2}\pi M_W^2 s_W^2}{\hat{s}^2 e^2 v^2 c_W^2} , \qquad \left\lvert \frac{f_{M_3}}{\Lambda^4} \right\rvert \leq \frac{256\sqrt{2}\pi M_W^2 s_W^2}{\hat{s}^2 e^2 v^2 c_W^2} ,$$

$$\left\lvert \frac{f_{M_4}}{\Lambda^4} \right\rvert \leq \frac{128\sqrt{2}\pi M_W^2 s_W}{\hat{s}^2 e^2 v^2 c_W} , \qquad \left\lvert \frac{f_{M_5}}{\Lambda^4} \right\rvert \leq \frac{256\sqrt{2}\pi M_W^2 s_W}{\hat{s}^2 e^2 v^2 c_W} ,$$

$$\left\lvert \frac{f_{M_7}}{\Lambda^4} \right\rvert \leq \frac{1024\sqrt{2}\pi M_W^2}{\hat{s}^2 e^2 v^2} , \qquad (4)$$

$$\left\lvert \frac{f_{T_0}}{\Lambda^4} \right\rvert \leq \frac{8\sqrt{2}\pi}{\hat{s}^2 s_W^2} , \qquad \left\lvert \frac{f_{T_1}}{\Lambda^4} \right\rvert \leq \frac{24\sqrt{2}\pi}{\hat{s}^2 s_W^2} ,$$

$$\left\lvert \frac{f_{T_2}}{\Lambda^4} \right\rvert \leq \frac{32\sqrt{2}\pi}{\hat{s}^2 s_W^2} , \qquad \left\lvert \frac{f_{T_5}}{\Lambda^4} \right\rvert \leq \frac{8\sqrt{2}\pi}{\hat{s}^2 c_W^2} ,$$

$$\left\lvert \frac{f_{T_6}}{\Lambda^4} \right\rvert \leq \frac{24\sqrt{2}\pi}{\hat{s}^2 c_W^2} , \qquad \left\lvert \frac{f_{T_7}}{\Lambda^4} \right\rvert \leq \frac{32\sqrt{2}\pi}{\hat{s}^2 c_W^2} ,$$

where $\sqrt{\hat{s}}$ is the c.m. energy of the subprocess and must be less equal to $\sqrt{s}$. Therefore, the strongest constraints can be obtained by using $\sqrt{s}$ instead of $\sqrt{\hat{s}}$ in Eq. (4), and the numerical results at $\sqrt{s} = 3$ and 10 TeV are listed in Table 1.

3 The event selection strategy of NLOF

The searching for NP signals at a high luminosity collider involves sifting through vast datasets to identify a small number of anomalous events. The LOF is an algorithm designed to find a small number of anomalous events based on density. Therefore, it is reasonable to expect that the LOF is suitable for the search of NP. Apart from this, since LOF algorithm is based on density, it also suits the nested AD (NAD) event selection strategy proposed in Ref. [27] which is useful when the interference between the SM and NP is important.

The core in the calculation of (N)LOF is to compute the distances. In the case of phenomenological studies in HEP, there are different ways to define the distance between two events (denoted as $d(A, B)$ where A and B are the points in the feature space to which the events A and B are mapped) [27, 86]. In this work, we use the Euclidean distance, i.e. $d(A, B)$ is the Euclidean distance between two points representing the two events in the feature space. However, the definition of $d(A, B)$ can be regarded as a kernel function, and different definitions may yield optimizations of the performance, and it can also be replaced by quantum kernels in future researches.

3.1 A brief introduction of LOF

LOF introduces a concept 'local reachability density' (LRD) which can be viewed as a measurement of density in its neighborhood. And a point is likely an outlier if its density is significantly smaller than the average density of its neighbors. To calculate LRD, LOF introduces a concept 'reachability distance' (LD) which can be viewed as an analog of distance. Then $LRD = 1/\overline{LD}$, where $\overline{LD}$ is the average of LD between the point and its neighbors. That is, if the point is far away from its neighbors, it is considered to be in a sparse region (low density region). The detailed procedure can be split as follows,

1. For a point A, compute its distance to its k-th nearest neighbor (denoted as $kd(A)$). Identify its k-nearest neighbors (denoted as $kNN(A)$).

2. For each neighbor of A (denoted as B), calculate the LD between them as $LD(A, B) = \max\{d(A, B), kd(B)\}$.

3. For A and its neighbors, compute their LRD as, $LRD(A) = k / \sum_{B \in kNN(A)} LD(A, B)$.

4. Calculate the LOF score (denoted as a) as $a(A) = \left(\sum_{B \in kNN(A)} LRD(B)/k \right) / LRD(A)$.

After the anomaly score a is obtained, one can use $a > a_{th}$ as a criterion to select NP signal events, where a_{th} is a tunable threshold. In LOF, there is another tunable parameter k, both the choice of k and a_{th} which will be discussed in the next section.

3.2 Using NLOF to search for aQGCs

In the relatively low energy region, the difference between the kinematic characteristics of the signaling event and the SM becomes less significant. In this scenario, finding NP signals is no longer a problem of AD. The NLOF selection event strategy is introduced to address this problem. Since the anomaly score computed by the LOF algorithm can be regarded as

a measure of the density of events in the feature space, it can be inferred that the anomaly score can also be used to measure changes in density, which is the idea of NAD. In NAD, one constructs a reference of anomaly scores based on the SM background events, and uses the changes of anomaly scores to select events which are obtained by comparing with the reference set. The NLOF event selection strategy can be summarized as follows,

1. Using the dataset obtained from MC simulations of the SM as the training dataset (denoted as S_r), the LOF applied to obtain the anomaly score for each event, denoted as a_r.

2. For the dataset to be investigated (it can be from the MC simulation or from the experiments, denoted as S_i), the LOF is again applied to obtain the anomaly score for each event, denoted a_i.

3. For each event in S_i, find the nearest neighbor event in S_r and calculate the change in the anomaly score as $\Delta a = a_i - a_r$.

After Δa is obtained, one can use $|\Delta a| > \Delta a_{th}$ as a criterion to select NP signal events.

4 Numerical result

4.1 Data preparation

The events are generated by scanning in the coefficient space within unitarity bounds and the constraints obtained at 95% C.L. at the LHC. The constraints at the LHC for $O_{M_{0,1,7}}$ operators are tight (the constraints in Ref. [71] are one order of magnitude than the unitarity bounds in Table 1), and the signals at the $\sqrt{s} = 3$ (TeV) can be hardly observed if we use the range of the coefficients at the LHC, and therefore these operators are not studied in this work. When the unitarity bounds are tighter, we use the range in Table 1, otherwise, we use the coefficient ranges listed in Table 2. The simulation is carried out with the help of the MC simulation toolkits `MadGraph5@NLO` [88–90]. A fast detector simulation is applied by using the `Delphes` [91] with the default muon collider card. The signal and background events are prepared using `MLAnalysis` [92], and the anomaly scores are calculated using the LOF algorithm in `scikit-learn` [93]. Since the unitarity bounds are strong for the O_{M_i} operators

Table 2: The range of coefficients in the case where the partial wave unitarity bounds are looser than the constraints at the LHC.

$\sqrt{s}$	3 TeV
$\left\|f_{M_3}/\Lambda^4\right\|$ (TeV^{-4})	$[-2.7, 2.7]$ [74]
$\left\|f_{M_4}/\Lambda^4\right\|$ (TeV^{-4})	$[-3.7, 3.6]$ [74]
$\left\|f_{M_5}/\Lambda^4\right\|$ (TeV^{-4})	$[-8.3, 8.3]$ [87]
$\left\|f_{T_0}/\Lambda^4\right\|$ (TeV^{-4})	$[-0.12, 0.11]$ [71]
$\left\|f_{T_1}/\Lambda^4\right\|$ (TeV^{-4})	$[-0.12, 0.13]$ [71]
$\left\|f_{T_2}/\Lambda^4\right\|$ (TeV^{-4})	$[-0.28, 0.28]$ [71]
$\left\|f_{T_5}/\Lambda^4\right\|$ (TeV^{-4})	$[-0.31, 0.33]$ [74]
$\left\|f_{T_6}/\Lambda^4\right\|$ (TeV^{-4})	$[-0.25, 0.27]$ [74]
$\left\|f_{T_7}/\Lambda^4\right\|$ (TeV^{-4})	$[-0.67, 0.73]$ [74]

at $\sqrt{s} = 10$ TeV, and there are few signal events when scanning the coefficients within the limit of the unitarity bounds, or a larger number of background evens is needed, for simplicity, at $\sqrt{s} = 10$ TeV only O_{T_i} operators are considered.

Since the muon collider is a future collider, at this stage the effect of the detector can only be estimated using simulation. In this work, we choose the default muon collider card in `Delphes`. That means, the results are purely statistical and do not include detector systematics or beam-induced backgrounds. Denoting E_γ and η_γ as the energy and pseudo-rapidity of a photon, the photon efficiency is 94% when $E_\gamma \geq 2$ GeV and $|\eta_\gamma| < 0.7$, and 90% when $E_\gamma \geq 2$ GeV and $2.5 \geq |\eta_\gamma| \geq 0.7$, and otherwise zero. The photon is considered as isolated when $\sum p_T / p_T^\gamma < 0.2$ where the sum runs over other particles in the vicinity of the photon with $\Delta R < 0.1$ and with $p_T > 0.5$ GeV, where p_T is the transverse momentum, and $\Delta R = \sqrt{\Delta\eta^2 + \Delta\phi^2}$ where $\Delta\eta$ and $\Delta\phi$ are differences of pseudo-rapidities and azimuth angles of two particles. The photon energy resolution is parameterized as $\sigma(E_\gamma)/E_\gamma = \sqrt{(1\%)^2 + (st^2/\sqrt{E_\gamma})}$, with st denoting the stochastic term varying across three pseudo-rapidity regions: 15.6% for $|\eta| \leq 0.78$, 17.5% for $0.78 < |\eta| \leq 0.83$, and 15.1% for $0.83 < |\eta| \leq 2.5$. We expect that, as machine learning algorithms, LOF/NLOF are insensitive to these parameters.

For the purpose of investigating the signal events, it is required that the final state contains at least two photons. The axes of the feature space are chosen to be five observables including E_{γ_1}, $p_{\gamma_1}^T$, E_{γ_2}, $p_{\gamma_2}^T$ and $m_{\gamma\gamma}$, where $E_{\gamma_{1,2}}$ are the energies of the hardest and the second hardest photons, $p_{\gamma_{1,2}}^T$ are the transverse momenta of them, and $m_{\gamma\gamma}$ is the invariant mass of them. By neglecting the effect of the detector simulation, except for the azimuth angles the information of the momenta of photons as well as the missing momentum can be reproduced by these five observables. As a ML algorithm, the NLOF is expected to automatically adapt to different feature spaces, which exhibit no fundamental performance differences but demonstrate variations in discriminability. All components of momenta are also tested as the feature space, producing comparable results with reduced computational efficiency. These five variables are selected for optimized computational cost. In order to reduce the 12-dimensional feature space to 5 dimensions, we analyzed the final state and selected five observables as the feature space. Such dimensionality reduction can, in fact, be achieved in a process-agnostic manner using ML algorithms, automatically and without the need to analyze the underlying physics. For instance, autoencoders or principle component analysis (PCA) can be employed for data dimensionality reduction. Since the main computational cost of the LOF/NLOF algorithm lies in calculating distances, it can be anticipated that applying dimensionality reduction and implementing LOF/NLOF in the latent space will significantly reduce computational complexity and improve the algorithm's operational efficiency. For complex processes with a large number of final-state particles, where manual analysis for dimensionality reduction becomes particularly intricate, this approach is especially meaningful. After dimensionality reduction, the z-score standardization [94] is applied to these observables, namely, $\hat{p}_i = (p_i - \bar{p}_i)/\epsilon_i$, where p_i denotes the i-th observable of an event, $\bar{p}_i$, ϵ_i are the average and standard deviation of p_i over the SM dataset. Then the feature space is a five-dimensional space composed of these five observables after the z-score standardization. An event (the j-th event) can be mapped to a point in this five-dimensional feature space as $\{\hat{p}_i^j\}$.

4.2 Compare the LOF with NLOF

Although LOF is inherently designed for exploring anomalous signals such as the ones from the NP, we find that it struggles to confine the expected coefficients within the partial wave unitarity bounds. Taking the case where LOF demonstrates relatively good performance as an example, we present a comparative analysis between LOF and NLOF for O_{M_2} at $\sqrt{s} = 3$ TeV.
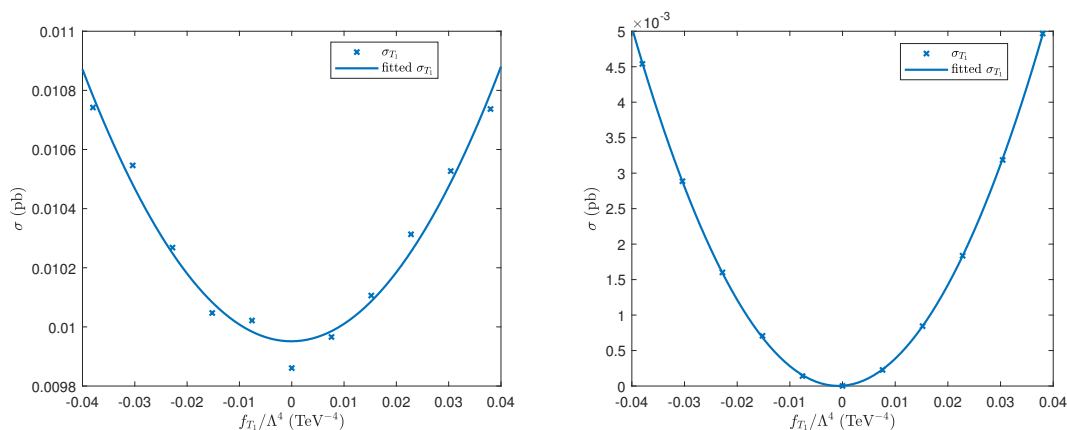
Figure 2: Fitted cross sections after cut using the LOF (the left panel) and the NLOF (the right panel) algorithms at $\sqrt{s} = 10$ TeV for O_{T_1}.

We tried all three cases with $k = 500$, 1000 and 2000, and the NLOF rendering is best at $k = 2000$. And it is the LOF rendering that is best at $k = 2000$, so in the use of NLOF and LOF two algorithms are taken $k = 2000$ respectively. Results with different choices of k and thresholds will be discussed in the next subsection.

After scanning the coefficient space, the anomaly scores a are calculated, then a cut $a > a_{th} = 1.5$ (optimized for the signal significance) is applied. With interference between the SM and NP considered, the cross section after cut is,

$$\sigma(f) = \sigma_{SM} + f\sigma_{int} + f^2\sigma_{NP}, \tag{5}$$

where f is the operator coefficient, σ_{SM}, σ_{int} and σ_{NP} are parameters to be fitted representing the contribution from the SM, the interference, and the NP alone, respectively.

The fitting of the cross section after cut in the case of LOF is shown in the left panel of Fig. 2. For NLOF, after selecting the events with $\Delta a > \Delta a_{th} = 0.08$ (optimized for the signal significance), the cross section is also fitted according to Eq. (5), the result is shown in the right panel of Fig. 2. It can be seen that for the case of NLOF, the signal is more significant.

The expected coefficient constraints can be estimated using the signal significance defined as [95, 96],

$$\mathcal{S}_{stat} = \sqrt{2\left[(N_{bg} + N_s)\ln(1 + N_s/N_{bg}) - N_s\right]}, \tag{6}$$

where N_{bg} is the event numbers of the background and N_s is the event numbers of the signal, $N_{bg} = \sigma_{SM}L$ and $N_s = \left(f\sigma_{int} + f^2\sigma_{NP}\right)L$, where f is the constraint to be solved, σ_{SM}, σ_{int}, and σ_{NP} are the parameters fitted according to Eq. (5), and L is the luminosity. The expected constraints at 2σ, 3σ and 5σ can be obtained by solving the equations $\mathcal{S}_{stat} = 2, 3$ and 5.

At $\sqrt{s} = 3$ TeV the designed luminosity is $L = 1$ ab [97, 98]. The expected coefficient constraints at $S_{stat} = 2$ are $[-1.12, 1.19]$ (TeV^{-4}) in the case of LOF, and $[-0.267, 0.284]$ (TeV^{-4}) in the case of NLOF. It can be seen that, the NLOF can outperform the LOF by one order of magnitude.

4.3 Expected constraints on the coefficients

The expected constraints in the cases of O_M operators at $\sqrt{s} = 3$ TeV and O_T operators at both $\sqrt{s} = 3$ TeV and $\sqrt{s} = 10$ TeV are studied. The Δa_{th} are chosen as 0.08 at $\sqrt{s} = 3$ TeV and 0.8 at $\sqrt{s} = 10$ TeV, respectively. It has been introduced that, the thresholds of the anomaly

scores to select the events are optimized for signal significance. As an example, the expected constraints on O_{T_1} at $\sqrt{s} = 10$ TeV as a function of Δa_{th} is shown in Fig. 3. The fittings of the cross sections after cuts are shown in Figs. 4 and 5. The cross sections for the cases of O_{M_3} and O_{M_4} are close to each other due to the accident that, at leading order of M_Z^2/s, the NP contributions for the two cases are $\sigma_{O_{M_3}}/\sigma_{O_{M_4}} = 17c_W^2/(60s_W^2) \approx 1$ [24]. The expected constraints on the coefficients obtained using signal significance are shown in Tables 3 and 4.

In addition to different thresholds, the selection of different k-values also influences the results. In Table 5, we present a comparison of results for $k = 500, 1000,$ and 2000. It can be observed that larger k-values yield tighter coefficient constraints. Even larger k-values are not considered due to computational resource limitations. However, based on the comparison in Table 5, it can be inferred that the sensitivity of the coefficient constraints to k is moderate.
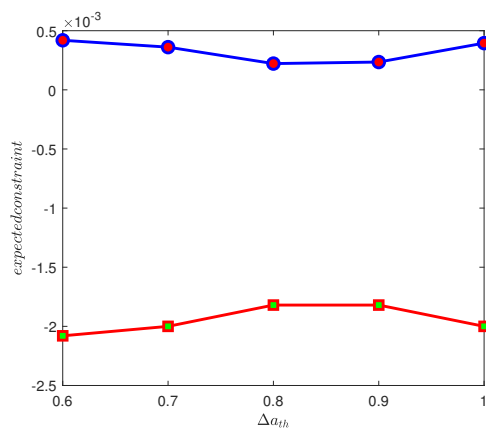
Figure 3: Expected constraint on the coefficient f_{T_1}/Λ^4 as a function of Δa_{th} for the NLOF at $\sqrt{s} = 10$ TeV.
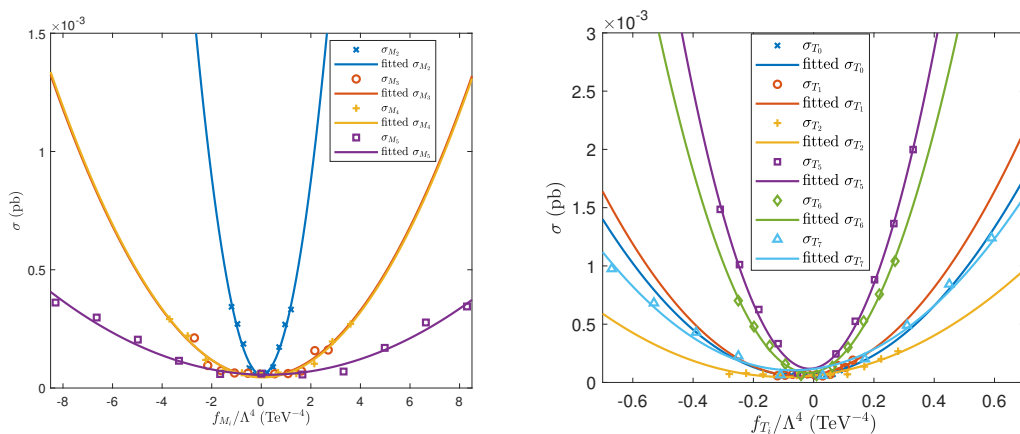
Figure 4: Fitted cross sections after cut at $\sqrt{s} = 3$ TeV for $O_{M_{2,3,4}}$ (the left panel) and $O_{T_{0,1,2,5,6,7}}$ (the right panel).
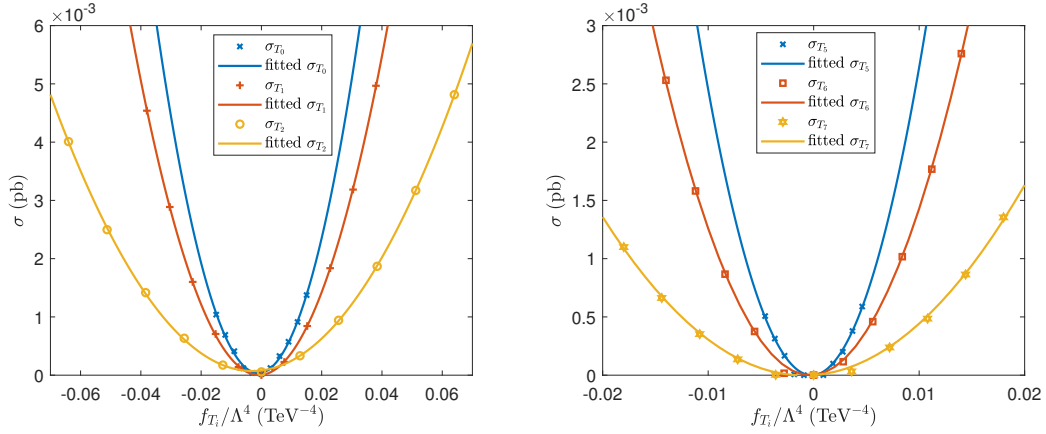
Figure 5: Fitted cross sections after cut at $\sqrt{s} = 3$ TeV for $O_{T_{0,1,2}}$ (the left panel) and $O_{T_{5,6,7}}$ (the right panel).

4.4 Comparison of NLOF with other methods

In Ref. [24] the signals of aQGCs in the process $\mu^+ \mu^- \to \gamma\gamma\nu\bar{\nu}$ at $\sqrt{s} = 10$ TeV were also considered, but with the interference terms ignored, with a kmeans AD (KMAD) algorithm and a quantum kernel KMAD (QKMAD) algorithm. To compare our method with QKMAD, we use the operator O_{T_1} at $\sqrt{s} = 10$ TeV and $S_{stat} = 2$ as an example. A traditional event selection strategy is also included in the comparison, which is,

$$p_{\gamma_1}^T > 2.2 \text{ TeV}, \quad p_{\gamma_2}^T < 0.8 \text{ TeV}, \quad m_{\gamma\gamma} > 1 \text{ TeV}. \tag{7}$$

Table 3: Projected sensitivity the coefficients of the $O_{M_{2,3,4}}$ and $O_{T_{0,1,2,5,6,7}}$ operators at $\sqrt{s} = 3$ TeV.

	S_{stat}	3 TeV 1 ab^{-1} (TeV^{-4})		S_{stat}	3 TeV 1 ab^{-1} (TeV^{-4})
$\frac{f_{M_2}}{\Lambda^4}$	2	$[-0.267, 0.284]$	$\frac{f_{M_3}}{\Lambda^4}$	2	$[-0.898, 0.912]$
	3	$[-0.333, 0.349]$		3	$[-1.11, 1.13]$
	5	$[-0.440, 0.457]$		5	$[-1.47, 1.48]$
$\frac{f_{M_4}}{\Lambda^4}$	2	$[-0.845, 0.940]$	$\frac{f_{M_5}}{\Lambda^4}$	2	$[-1.64, 2.07]$
	3	$[-1.06, 1.15]$		3	$[-2.07, 2.51]$
	5	$[-1.41, 1.50]$		5	$[-2.79, 3.22]$
$\frac{f_{T_0}}{\Lambda^4}$	2	$[-0.124, 0.0415]$	$\frac{f_{T_1}}{\Lambda^4}$	2	$[-0.134, 0.0333]$
	3	$[-0.139, 0.0565]$		3	$[-0.147, 0.0464]$
	5	$[-0.165, 0.0825]$		5	$[-0.170, 0.0693]$
$\frac{f_{T_2}}{\Lambda^4}$	2	$[-0.231, 0.0471]$	$\frac{f_{T_5}}{\Lambda^4}$	2	$[-0.0533, 0.0265]$
	3	$[-0.251, 0.0665]$		3	$[-0.0617, 0.0348]$
	5	$[-0.285, 0.101]$		5	$[-0.0756, 0.0487]$
$\frac{f_{T_6}}{\Lambda^4}$	2	$[-0.0620, 0.0261]$	$\frac{f_{T_7}}{\Lambda^4}$	2	$[-0.183, 0.0479]$
	3	$[-0.0708, 0.0348]$		3	$[-0.201, 0.0663]$
	5	$[-0.0855, 0.0496]$		5	$[-0.233, 0.0981]$

Table 4: Same as Table 3 but for $\sqrt{s} = 10$ TeV.

	S_{stat}	10 TeV 10 ab^{-1} (10^{-4}TeV^{-4})		S_{stat}	10 TeV 10 ab^{-1} (10^{-4}TeV^{-4})
$\frac{f_{T_0}}{\Lambda^4}$	2	$[-13.2, 0.510]$	$\frac{f_{T_1}}{\Lambda^4}$	2	$[-18.2, 2.22]$
	3	$[-13.5, 0.820]$		3	$[-19.2, 3.23]$
	5	$[-14.2, 1.51]$		5	$[-21.1, 5.12]$
$\frac{f_{T_2}}{\Lambda^4}$	2	$[-67.5, 8.03]$	$\frac{f_{T_5}}{\Lambda^4}$	2	$[-3.98, 0.265]$
	3	$[-71.0, 11.5]$		3	$[-4.13, 0.420]$
	5	$[-77.3, 17.8]$		5	$[-4.46, 0.753]$
$\frac{f_{T_6}}{\Lambda^4}$	2	$[-6.96, 0.658]$	$\frac{f_{T_7}}{\Lambda^4}$	2	$[-18.9, 0.599]$
	3	$[-7.29, 0.988]$		3	$[-19.3, 0.941]$
	5	$[-7.95, 1.64]$		5	$[-20.0, 1.69]$

Table 5: When k = 500, 1000 and 2000, under the condition of $\sqrt{s} = 10$ TeV,Projected sensitivity the coefficients of the O_{T_1} operators.

k		S_{stat}	10 TeV 10 ab^{-1} (10^{-4}TeV^{-4})
500	$\frac{f_{T_1}}{\Lambda^4}$	2	$[-20.1, 5.17]$
		3	$[-22.0, 7.13]$
		5	$[-25.4, 10.5]$
1000	$\frac{f_{T_1}}{\Lambda^4}$	2	$[-20.0, 4.49]$
		3	$[-21.8, 6.26]$
		5	$[-24.9, 9.35]$
2000	$\frac{f_{T_1}}{\Lambda^4}$	2	$[-18.2, 2.22]$
		3	$[-19.2, 3.23]$
		5	$[-21.1, 5.12]$

The fitting of the traditional event selection strategy is compared with NLOF in Fig. 6, it can be shown that the NLOF can preserve more signal events while suppressing the background events to a similar amplitude as the traditional event selection strategy.

Isolation forest (IF) was used in Ref. [99] to study the signals of aQGCs in VBS processes at the LHC. Nested IF (NIF) was employed in Ref. [27] to investigate the signals of neutral triple gauge couplings (nTGCs) in diboson processes at the CEPC. In this work, we also utilize IF and NIF to study the O_{T_1} operator in the process $\mu^+\mu^- \to \gamma\gamma\nu\bar{\nu}$ at $\sqrt{s} = 10$ TeV. The same dataset is used, and the forest consists of 100 trees. For IF, we select the events with $\Delta a > \Delta a_{th} = 0.6$ (optimized for the signal significance), where a is the anomaly score in the sense of IF. For NIF, we select the events with $\Delta a > \Delta a_{th} = 0.05$ (optimized for the signal significance), where Δa is the change of anomaly score in the sense of NIF. The cross sections after cuts, along with the fittings are shown in Fig. 7. The expected coefficient constraint calculated by the traditional event selection strategy is $[-1.73 \times 10^{-3}, 6.15 \times 10^{-4}]$ (TeV^{-4}), by the NLOF algorithm is $[-1.82 \times 10^{-3}, 2.22 \times 10^{-4}]$ (TeV^{-4}), by the IF algorithm is $[-3.84 \times 10^{-3}, 2.15 \times 10^{-3}]$ (TeV^{-4}),by the NIF algorithm is $[-2.34 \times 10^{-3}, 4.38 \times 10^{-4}]$(TeV^{-4}),
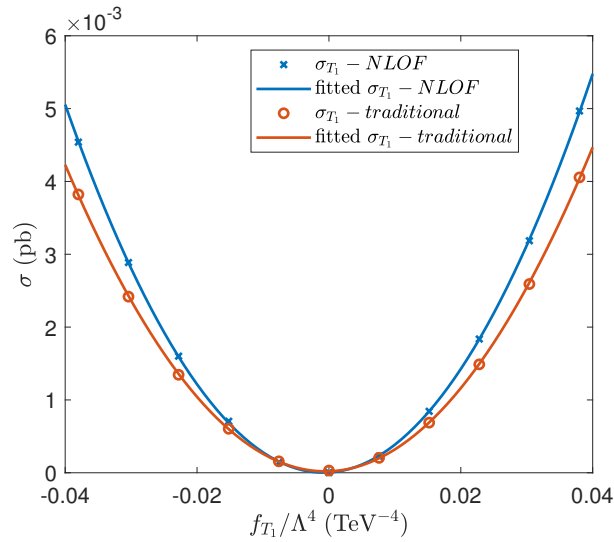
Figure 6: Comparison of the cross section after cut between the case of a traditional event selection strategy and the NLOF for O_{T_1} at $\sqrt{s} = 10$ TeV.
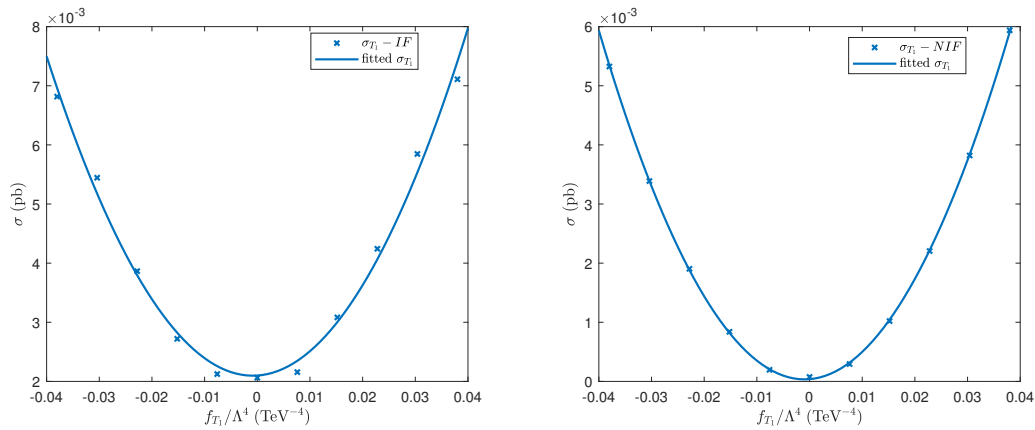
Figure 7: Same as Fig. 2 but for the IF (the left panel) and the NIF (the right panel).

by KMAD is $[-1.66 \times 10^{-3}, 1.66 \times 10^{-3}]$ (TeV^{-4}), and by QKMAD is $[-1.65 \times 10^{-3}, 1.65 \times 10^{-3}]$ (TeV^{-4}). It can be seen that the expected coefficient constraint of the NLOF algorithm is the tightest among all methods. The comparison of the above mentioned methods is shown in the left panel of Fig. 8.

To make the comparison more transparent, and to study the impact of developing event selection criteria using only background events, the results at fixed background acceptance levels are investigated. Taking the O_{T_1} at 10 TeV as an example, the cases are considered when 1%, 5% and 10% background events are preserved. The cross sections after cuts, along with the fittings are shown in Fig. 9. For the cases of 1% with LOF, and 10% with NIF, the cross sections cannot be well fitted, and the results are not shown. For NLOF, the expected constraints at $S_{stat} = 2$ are $[-3.66 \times 10^{-3}, 1.36 \times 10^{-3}]$ (TeV^{-4}), $[-4.67 \times 10^{-3}, 2.28 \times 10^{-3}]$ (TeV^{-4}) and $[-2.25 \times 10^{-3}, 2.83 \times 10^{-3}]$ (TeV^{-4}), for the cases of 1%, 5% and 10%, respectively. As can be seen, the obtained coefficient constraints exhibit a span comparable in magnitude to the case when the optimal Δa_{th} is chosen, demonstrating the feasibility of the NLOF with infor-

mation of only background events. However, the coefficient constraints obtained in this way are systematically less stringent. As a comparison, the coefficient constraints for the cases of 1%, 5% and 10% background efficiencies obtained by traditional method, LOF, IF, and NIF are shown in the right panel of Fig. 8. The NLOF is the tightest among all cases.
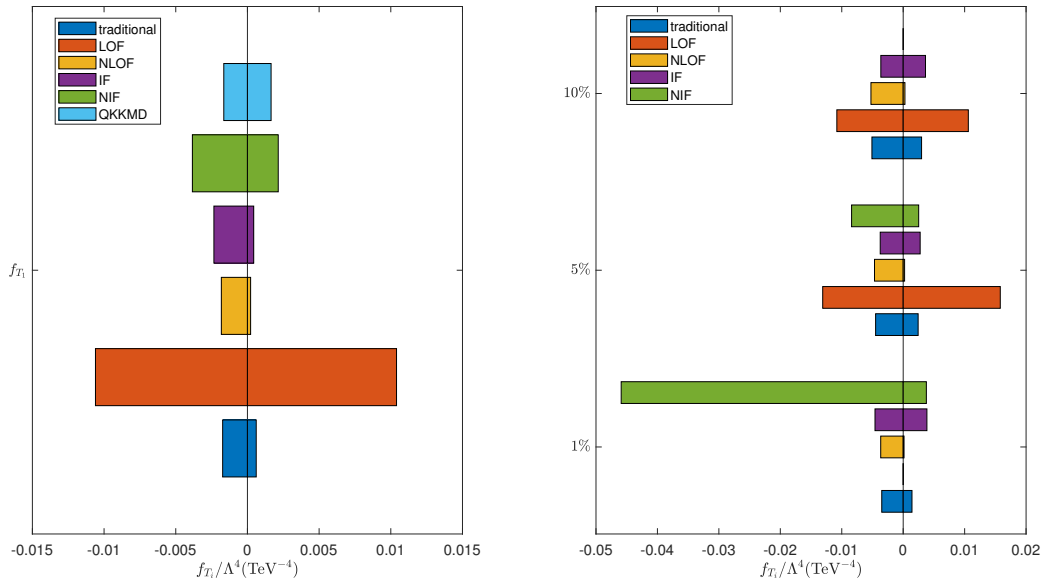
Figure 8: The left figure shows the comparison of the expected coefficient constraint when $S_{stat} = 2$ for O_{T_1} at $\sqrt{s} = 10$ TeV obtained by traditional methods, LOF, NLOF, IF, NIF, and QKKMD when the event selection strategies are optimized according to signal significance. The right figure shows the comparison of the expected coefficient constraint when $S_{stat} = 2$ for O_{T_1} at $\sqrt{s} = 10$ TeV obtained by traditional methods, LOF, NLOF, IF, and NIF when the background is suppressed to 1%, 5%, and 10%. For the cases of 1% with LOF, and 10% with NIF, the cross sections cannot be well fitted, and the results are not shown.
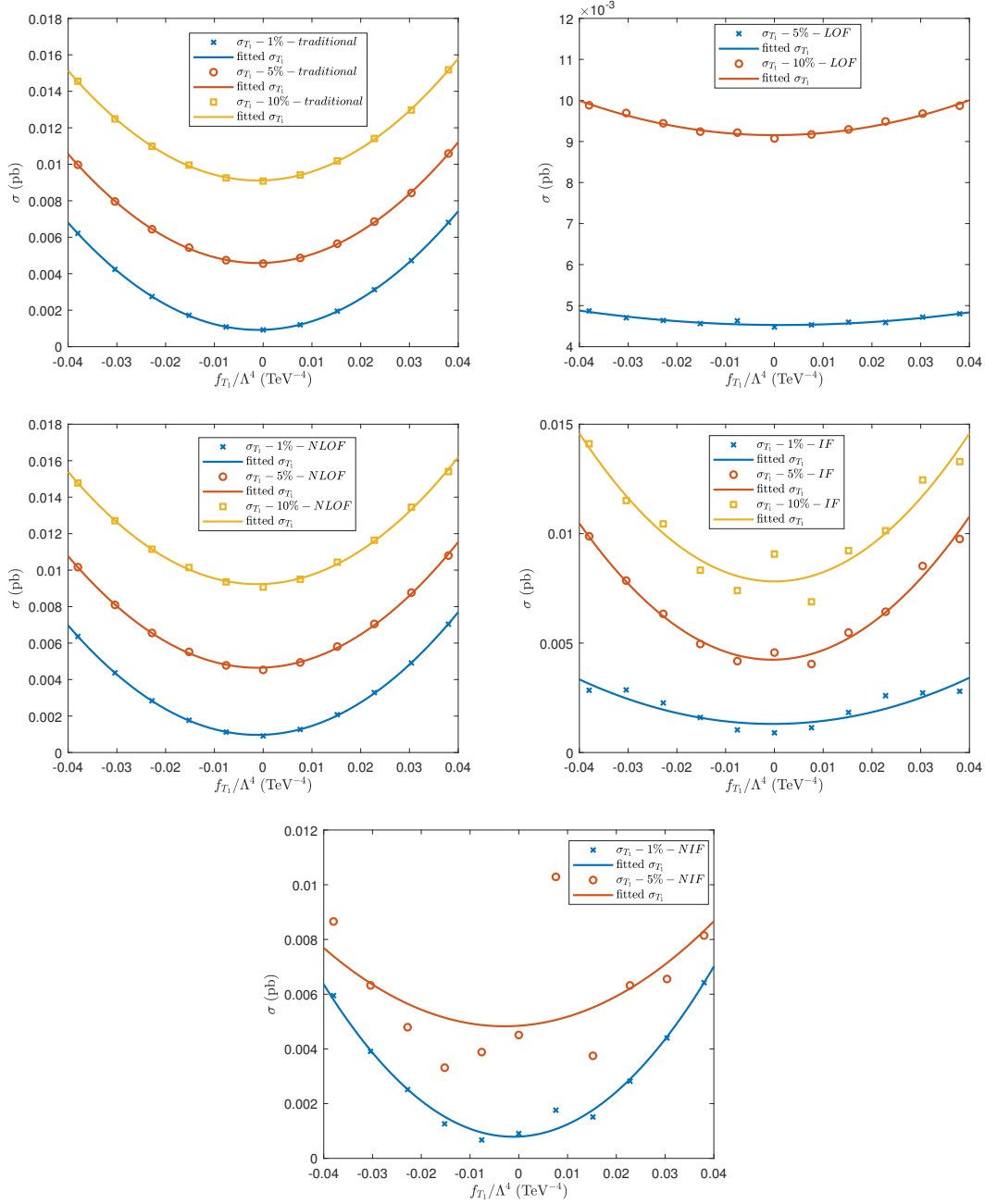
Figure 9: Taking the case of O_{T_1} at $\sqrt{s} = 10$ TeV as an example, the fitted cross sections after cuts with the traditional methods (the left panel in the first row), LOF (the right panel in the first row), NLOF (the left panel in the second row), IF (the right panel in the second row), and NIF (the panel in the third row), when the background efficiency is fixed to 1%, 5%, and 10%. For the cases of 1% with LOF, and 10% with NIF, the cross sections cannot be well fitted, and the results are not shown.

5 Summary

In recent years, with the increasing luminosities of colliders, handling the growing amount of data has become a major challenge for future NP phenomenological research. To improve efficiency, ML algorithms have been introduced into the field of high-energy physics, including the the (N)LOF algorithms. This paper investigates how to search for NP signals using (N)LOF anomaly detection event selection strategy. Taking the process $\mu^+\mu^- \to \gamma\gamma\nu\bar{\nu}$ at muon colliders as an example, the dimension-8 operators contributing to aQGCs are studied. Expected coefficient constraints obtained using (N)LOF algorithm are presented.

The results indicate that, the VBS process $\mu^+\mu^- \to \gamma\gamma\nu\bar{\nu}$ at muon colliders is sensitive to the aQGCs. It can be concluded that, the (N)LOF can contribute to the search of signals from aQGCs. It is shown that the NLOF algorithm can improve the sensitivity of the search for aQGCs by about one order of magnitude compared to the traditional local outlier factor (LOF) algorithm. The expected coefficient constraints obtained using NLOF algorithm are shown to be tighter than KMAD, QKMAD, and a traditional counterpart.

In the case of $k \ll m$ and $d \ll m$, where m is the size of dataset, d is the dimension of feature space, with k-dimensional tree to calculate the k-nearest neighbors, the computational complexity to calculate the LOF anomaly scores of a dataset can be estimated as $\mathcal{O}(dm\log(m)) + \mathcal{O}(m\log m) + \mathcal{O}(mk)$. In the case of NLOF, two datasets are needed. Assuming m_1 is the size of test dataset, m_2 is the size of reference dataset (the SM background events). After calculating the anomaly scores of the two datasets, one needs to find for each point of test dataset, the nearest point in reference dataset to that point, where the computational complexity is $\mathcal{O}(d(m_1 + m_2)\log m_2)$. So, in the case of NLOF, the dominant cost is still the calculation of the anomaly scores, and the computational complexity is about $\mathcal{O}((d+1)m_1\log(m_1) + ((2d+2)m_2 + dm_1)\log(m_2))$ when $k \ll m_{1,2}$. Since the reference dataset is obtained from MC, and does not grow with the luminosities of the colliders, by assuming $m_2 \ll m_1$, the increasing of computational complexity is moderate to use NLOF instead of LOF.

As a density-based algorithm, the core computation in LOF primarily involves calculating point-to-point distances. Even when extended with nesting, as in the nested LOF (NLOF) algorithm proposed in this study, the computational backbone remains anchored in distance calculations. This grants both LOF and NLOF inherent flexibility, i.e., we can strategically define various kernel functions, precompute inter-point distances, and subsequently input them within (N)LOF frameworks. Notably, with the recent surge of quantum ML applications in NP searches, quantum computing, as a high-throughput data processing paradigm, enables ultra-efficient distance computation through quantum kernels. This naturally facilitates quantum-enhanced extensions, quantum kernel (N)LOF in the future.

Acknowledgments

Funding information This work was supported in part by the National Natural Science Foundation of China under Grants Nos. 11905093 and 12147214, and was supported in part by National Key R&D Program of China under Contracts No. 2022YFE0116900, and by the Natural Science Foundation of the Liaoning Scientific Committee Nos. JYTMS20231053 and LJKMZ20221431.

References

[1] A. Crivellin and B. Mellado, *Anomalies in particle physics and their implications for physics beyond the Standard Model*, Nat. Rev. Phys. **6**, 294 (2024), doi:10.1038/s42254-024-00703-6 [preprint doi:10.48550/arXiv.2309.03870].

[2] J. Ellis, *Outstanding questions: Physics beyond the Standard Model*, Philos. Trans. R. Soc. A: Math. Phys. Eng. Sci. **370**, 818 (2012), doi:10.1098/rsta.2011.0452.

[3] K. Albertsson et al., *Machine learning in high energy physics community white paper*, J. Phys.: Conf. Ser. **1085**, 022008 (2018), doi:10.1088/1742-6596/1085/2/022008 [preprint doi:10.48550/arXiv.1807.02876].

[4] D. Guest, K. Cranmer and D. Whiteson, *Deep learning and its application to LHC physics*, Annu. Rev. Nucl. Part. Sci. **68**, 161 (2018), doi:10.1146/annurev-nucl-101917-021019 [preprint doi:10.48550/arXiv.1806.11484].

[5] A. Radovic, M. Williams, D. Rousseau, M. Kagan, D. Bonacorsi, A. Himmel, A. Aurisano, K. Terao and T. Wongjirad, *Machine learning at the energy and intensity frontiers of particle physics*, Nature **560**, 41 (2018), doi:10.1038/s41586-018-0361-2.

[6] P. Baldi, P. Sadowski and D. Whiteson, *Searching for exotic particles in high-energy physics with deep learning*, Nat. Commun. **5**, 4308 (2014), doi:10.1038/ncomms5308 [preprint doi:10.48550/arXiv.1402.4735].

[7] J. Ren, L. Wu, J. M. Yang and J. Zhao, *Exploring supersymmetry with machine learning*, Nucl. Phys. B **943**, 114613 (2019), doi:10.1016/j.nuclphysb.2019.114613 [preprint doi:10.48550/arXiv.1708.06615].

[8] M. Abdughani, J. Ren, L. Wu and J. M. Yang, *Probing stop pair production at the LHC with graph neural networks*, J. High Energy Phys. **08**, 055 (2019), doi:10.1007/JHEP08(2019)055 [preprint doi:10.48550/arXiv.1807.09088].

[9] J. Ren, L. Wu and J. M. Yang, *Unveiling CP property of top-Higgs coupling with graph neural networks at the LHC*, Phys. Lett. B **802**, 135198 (2020), doi:10.1016/j.physletb.2020.135198 [preprint doi:10.48550/arXiv.1901.05627].

[10] M. Letizia, G. Losapio, M. Rando, G. Grosso, A. Wulzer, M. Pierini, M. Zanetti and L. Rosasco, *Learning new physics efficiently with nonparametric methods*, Eur. Phys. J. C **82**, 879 (2022), doi:10.1140/epjc/s10052-022-10830-y [preprint doi:10.48550/arXiv.2204.02317].

[11] R. T. D'Agnolo, G. Grosso, M. Pierini, A. Wulzer and M. Zanetti, *Learning multivariate new physics*, Eur. Phys. J. C **81**, 89 (2021), doi:10.1140/epjc/s10052-021-08853-y [preprint doi:10.48550/arXiv.1912.12155].

[12] R. T. D'Agnolo and A. Wulzer, *Learning new physics from a machine*, Phys. Rev. D **99**, 015014 (2019), doi:10.1103/PhysRevD.99.015014 [preprint doi:10.48550/arXiv.1806.02350].

[13] A. De Simone and T. Jacques, *Guiding new physics searches with unsupervised learning*, Eur. Phys. J. C **79**, 289 (2019), doi:10.1140/epjc/s10052-019-6787-3 [preprint doi:10.48550/arXiv.1807.06038].

[14] M. A. Md Ali, N. Badrud'din, H. Abdullah and F. Kemi, *Alternate methods for anomaly detection in high-energy physics via semi-supervised learning*, Int. J. Mod. Phys. A **35**, 2050131 (2020), doi:10.1142/S0217751X20501316.

[15] E. Fol, R. Tomás, J. Coello de Portugal and G. Franchetti, *Detection of faulty beam position monitors using unsupervised learning*, Phys. Rev. Accel. Beams **23**, 102805 (2020), doi:10.1103/PhysRevAccelBeams.23.102805.

[16] G. Kasieczka et al., *The LHC Olympics 2020 a community challenge for anomaly detection in high energy physics*, Rep. Prog. Phys. **84**, 124201 (2021), doi:10.1088/1361-6633/ac36b9 [preprint doi:10.48550/arXiv.2101.08320].

[17] Y.-F. Dong, Y.-C. Mao and J.-C. Yang, *Searching for anomalous quartic gauge couplings at muon colliders using principal component analysis*, Eur. Phys. J. C **83**, 555 (2023), doi:10.1140/epjc/s10052-023-11719-0 [preprint doi:10.48550/arXiv.2304.01505].

[18] M. Crispim Romão, N. F. Castro and R. Pedro, *Finding new physics without learning about it: Anomaly detection as a tool for searches at colliders*, Eur. Phys. J. C **81**, 27 (2021), doi:10.1140/epjc/s10052-020-08807-w [preprint doi:10.48550/arXiv.2006.05432].

[19] M. van Beekveld et al., *Combining outlier analysis algorithms to identify new physics at the LHC*, J. High Energy Phys. **09**, 024 (2021), doi:10.1007/JHEP09(2021)024 [preprint doi:10.48550/arXiv.2010.07940].

[20] M. Kuusela, T. Vatanen, E. Malmi, T. Raiko, T. Aaltonen and Y. Nagai, *Semi-supervised anomaly detection – Towards model-independent searches of new physics*, J. Phys.: Conf. Ser. **368**, 012032 (2012), doi:10.1088/1742-6596/368/1/012032 [preprint doi:10.48550/arXiv.1112.3329].

[21] Y.-T. Zhang, X.-T. Wang and J.-C. Yang, *Searching for gluon quartic gauge couplings at muon colliders using the autoencoder*, Phys. Rev. D **109**, 095028 (2024), doi:10.1103/PhysRevD.109.095028 [preprint doi:10.48550/arXiv.2311.16627].

[22] S. Zhang, J.-C. Yang and Y.-C. Guo, *Using k-means assistant event selection strategy to study anomalous quartic gauge couplings at muon colliders*, Eur. Phys. J. C **84**, 142 (2024), doi:10.1140/epjc/s10052-024-12494-2 [preprint doi:10.48550/arXiv.2302.01274].

[23] J.-C. Yang, S. Zhang and C.-X. Yue, *A quantum machine learning classifier to search for new physics*, (arXiv preprint) doi:10.48550/arXiv.2410.18847.

[24] S. Zhang, K.-X. Chen and J.-C. Yang, *Detect anomalous quartic gauge couplings at muon colliders with quantum kernel k-means*, Eur. Phys. J. C **85**, 378 (2025), doi:10.1140/epjc/s10052-025-14069-1 [preprint doi:10.48550/arXiv.2409.07010].

[25] S. Zhang, Y.-C. Guo and J.-C. Yang, *Optimize the event selection strategy to study the anomalous quartic gauge couplings at muon colliders using the support vector machine and quantum support vector machine*, Eur. Phys. J. C **84**, 833 (2024), doi:10.1140/epjc/s10052-024-13208-4 [preprint doi:10.48550/arXiv.2311.15280].

[26] M. M. Breunig, H.-P. Kriegel, R. T. Ng and J. Sander, *LOF*, ACM SIGMOD Rec. **29**, 93 (2000), doi:10.1145/335191.335388.

[27] J.-C. Yang, Y.-C. Guo and L.-H. Cai, *Using a nested anomaly detection machine learning algorithm to study the neutral triple gauge couplings at an e^+e^- collider*, Nucl. Phys. B **977**, 115735 (2022), doi:10.1016/j.nuclphysb.2022.115735 [preprint doi:10.48550/arXiv.2111.10543].

[28] S. Willenbrock and C. Zhang, *Effective field theory beyond the Standard Model*, Annu. Rev. Nucl. Part. Sci. **64**, 83 (2014), doi:10.1146/annurev-nucl-102313-025623 [preprint doi:10.48550/arXiv.1401.0470].

[29] E. Massó, *An effective guide to beyond the Standard Model physics*, J. High Energy Phys. **10**, 128 (2014), doi:10.1007/JHEP10(2014)128 [preprint doi:10.48550/arXiv.1406.6376].

[30] B. Grzadkowski, M. Iskrzyński, M. Misiak and J. Rosiek, *Dimension-six terms in the Standard Model Lagrangian*, J. High Energy Phys. **10**, 085 (2010), doi:10.1007/JHEP10(2010)085 [preprint doi:10.48550/arXiv.1008.4884].

[31] I. Brivio and M. Trott, *The Standard Model as an effective field theory*, Phys. Rep. **793**, 1 (2019), doi:10.1016/j.physrep.2018.11.002 [preprint doi:10.48550/arXiv.1706.08945].

[32] W. Buchmüller and D. Wyler, *Effective Lagrangian analysis of new interactions and flavour conservation*, Nucl. Phys. B **268**, 621 (1986), doi:10.1016/0550-3213(86)90262-2 [preprint doi:10.48550/arXiv.1105.3756].

[33] S. Weinberg, *Baryon- and lepton-nonconserving processes*, Phys. Rev. Lett. **43**, 1566 (1979), doi:10.1103/PhysRevLett.43.1566.

[34] D. Buttazzo, D. Redigolo, F. Sala and A. Tesi, *Fusing vectors into scalars at high energy lepton colliders*, J. High Energy Phys. **11**, 144 (2018), doi:10.1007/JHEP11(2018)144 [preprint doi:10.48550/arXiv.1807.04743].

[35] J. P. Delahaye, M. Diemoz, K. Long, B. Mansoulié, N. Pastrone, L. Rivkin, D. Schulte, A. Skrinsky and A. Wulzer, *Muon colliders*, (arXiv preprint) doi:10.48550/arXiv.1901.06150.

[36] A. Costantini, F. De Lillo, F. Maltoni, L. Mantani, O. Mattelaer, R. Ruiz and X. Zhao, *Vector boson fusion at multi-TeV muon colliders*, J. High Energy Phys. **09**, 080 (2020), doi:10.1007/JHEP09(2020)080 [preprint doi:10.48550/arXiv.2005.10289].

[37] M. Lu, A. Michael Levin, C. Li, A. Agapitos, Q. Li, F. Meng, S. Qian, J. Xiao and T. Yang, *The physics case for an electron-muon collider*, Adv. High Energy Phys. 6693618 (2021), doi:10.1155/2021/6693618 [preprint doi:10.48550/arXiv.2010.15144].

[38] H. Al Ali et al., *The muon smasher's guide*, Rep. Prog. Phys. **85**, 084201 (2022), doi:10.1088/1361-6633/ac6678 [preprint doi:10.48550/arXiv.2103.14043].

[39] R. Palmer et al., *Muon collider design*, Nucl. Phys. B - Proc. Suppl. **51**, 61 (1996), doi:10.1016/0920-5632(96)00417-3.

[40] S. D. Holmes and V. D. Shiltsev, *12.2 muon collider*, in *Accelerators and colliders*, Springer, Berlin, Heidelberg, Germany, ISBN 9783642230523 (2013), doi:10.1007/978-3-642-23053-0_48 [preprint doi:10.48550/arXiv.1202.3803].

[41] W. Liu and K.-P. Xie, *Probing electroweak phase transition with multi-TeV muon colliders and gravitational waves*, J. High Energy Phys. **04**, 015 (2021), doi:10.1007/JHEP04(2021)015 [preprint doi:10.48550/arXiv.2101.10469].

[42] W. Liu, K.-P. Xie and Z. Yi, *Testing leptogenesis at the LHC and future muon colliders: A Z' scenario*, Phys. Rev. D **105**, 095034 (2022), doi:10.1103/PhysRevD.105.095034 [preprint doi:10.48550/arXiv.2109.15087].

[43] D. R. Green, P. Meade and M.-A. Pleier, *Multiboson interactions at the LHC*, Rev. Mod. Phys. **89**, 035008 (2017), doi:10.1103/RevModPhys.89.035008 [preprint doi:10.48550/arXiv.1610.07572].

[44] J. Chang, K. Cheung, C.-T. Lu and T.-C. Yuan, *WW scattering in the era of post-Higgs-boson discovery*, Phys. Rev. D **87**, 093005 (2013), doi:10.1103/PhysRevD.87.093005 [preprint doi:10.48550/arXiv.1303.6335].

[45] B. Alessandro et al., *Vector boson scattering: Recent experimental and theory developments*, Rev. Phys. **3**, 44 (2018), doi:10.1016/j.revip.2018.11.001 [preprint doi:10.48550/arXiv.1801.04203].

[46] C. Zhang and S.-Y. Zhou, *Positivity bounds on vector boson scattering at the LHC*, Phys. Rev. D **100**, 095003 (2019), doi:10.1103/PhysRevD.100.095003 [preprint doi:10.48550/arXiv.1808.00010].

[47] Q. Bi, C. Zhang and S.-Y. Zhou, *Positivity constraints on aQGC: Carving out the physical parameter space*, J. High Energy Phys. **06**, 137 (2019), doi:10.1007/JHEP06(2019)137 [preprint doi:10.48550/arXiv.1902.08977].

[48] J. Ellis and S.-F. Ge, *Constraining gluonic quartic gauge coupling operators with $gg \to \gamma\gamma$*, Phys. Rev. Lett. **121**, 041801 (2018), doi:10.1103/PhysRevLett.121.041801 [preprint doi:10.48550/arXiv.1802.02416].

[49] J. Ellis, N. E. Mavromatos and T. You, *Light-by-light scattering constraint on Born-Infeld theory*, Phys. Rev. Lett. **118**, 261802 (2017), doi:10.1103/PhysRevLett.118.261802 [preprint doi:10.48550/arXiv.1703.08450].

[50] J. Ellis, S.-F. Ge, H.-J. He and R.-Q. Xiao, *Probing the scale of new physics in the $ZZ\gamma$ coupling at e^+e^- colliders*, Chin. Phys. C **44**, 063106 (2020), doi:10.1088/1674-1137/44/6/063106 [preprint doi:10.48550/arXiv.1902.06631].

[51] J. Ellis, H.-J. He and R.-Q. Xiao, *Probing new physics in dimension-8 neutral gauge couplings at e^+e^- colliders*, Sci. China Phys. Mech. Astron. **64**, 221062 (2020), doi:10.1007/s11433-020-1617-3 [preprint doi:10.48550/arXiv.2008.04298].

[52] G. J. Gounaris, J. Layssac and F. M. Renard, *Off-shell structure of the anomalous Z and γ selfcouplings*, Phys. Rev. D **62**, 073012 (2000), doi:10.1103/PhysRevD.62.073012 [preprint doi:10.48550/arXiv.hep-ph/0005269].

[53] G. J. Gounaris, J. Layssac and F. M. Renard, *Signatures of the anomalous $Z\gamma$ and ZZ production at lepton and hadron colliders*, Phys. Rev. D **61**, 073013 (2000), doi:10.1103/PhysRevD.61.073013 [preprint doi:10.48550/arXiv.hep-ph/9910395].

[54] A. Senol, H. Denizli, A. Yilmaz, I. Turk Cakir, K. Y. Oyulmaz, O. Karadeniz and O. Cakir, *Probing the effects of dimension-eight operators describing anomalous neutral triple gauge boson interactions at FCC-hh*, Nucl. Phys. B **935**, 365 (2018), doi:10.1016/j.nuclphysb.2018.08.018 [preprint doi:10.48550/arXiv.1805.03475].

[55] C. Degrande, *A basis of dimension-eight operators for anomalous neutral triple gauge boson interactions*, J. High Energy Phys. **02**, 101 (2014), doi:10.1007/JHEP02(2014)101 [preprint doi:10.48550/arXiv.1308.6323].

[56] S. Jahedi and J. Lahiri, *Probing anomalous $ZZ\gamma$ and $Z\gamma\gamma$ couplings at the e^+e^- colliders using optimal observable technique*, J. High Energy Phys. **04**, 085 (2023), doi:10.1007/JHEP04(2023)085 [preprint doi:10.48550/arXiv.2212.05121].

[57] S. Jahedi, *Optimal estimation of dimension-8 neutral triple gauge couplings at the e^+e^- colliders*, J. High Energy Phys. **12**, 031 (2023), doi:10.1007/JHEP12(2023)031 [preprint doi:10.48550/arXiv.2305.11266].

[58] C. Zhang and S.-Y. Zhou, *Convex geometry perspective on the (Standard Model) effective field theory space*, Phys. Rev. Lett. **125**, 201601 (2020), doi:10.1103/PhysRevLett.125.201601 [preprint doi:10.48550/arXiv.2005.03047].

[59] ATLAS collaboration: G. Aad et al., *Evidence for electroweak production of $W^\pm W^\pm jj$ in pp collisions at $\sqrt{s} = 8$ TeV with the ATLAS detector*, Phys. Rev. Lett. **113**, 141803 (2014), doi:10.1103/PhysRevLett.113.141803 [preprint doi:10.48550/arXiv.1405.6241].

[60] A. M. Sirunyan et al., *Measurements of production cross sections of WZ and same-sign WW boson pairs in association with two jets in proton-proton collisions at $\sqrt{s} = 13$ TeV*, Phys. Lett. B **809**, 135710 (2020), doi:10.1016/j.physletb.2020.135710 [preprint doi:10.48550/arXiv.2005.01173].

[61] ATLAS collaboration: M. Aaboud et al., *Studies of $Z\gamma$ production in association with a high-mass dijet system in pp collisions at $\sqrt{s} = 8$ TeV with the ATLAS detector*, J. High Energy Phys. **07**, 107 (2017), doi:10.1007/JHEP07(2017)107 [preprint doi:10.48550/arXiv.1705.01966].

[62] V. Khachatryan et al., *Measurement of the cross section for electroweak production of $Z\gamma$ in association with two jets and constraints on anomalous quartic gauge couplings in proton–proton collisions at $\sqrt{s} = 8$ TeV*, Phys. Lett. B **770**, 380 (2017), doi:10.1016/j.physletb.2017.04.071 [preprint doi:10.48550/arXiv.1702.03025].

[63] CMS collaboration: A. M. Sirunyan et al., *Measurement of the cross section for electroweak production of a Z boson, a photon and two jets in proton-proton collisions at $\sqrt{s} = 13$ TeV and constraints on anomalous quartic couplings*, J. High Energy Phys. **06**, 076 (2020), doi:10.1007/JHEP06(2020)076 [preprint doi:10.48550/arXiv.2002.09902].

[64] CMS collaboration: V. Khachatryan et al., *Measurement of electroweak-induced production of $W\gamma$ with two jets in pp collisions at $\sqrt{s} = 8$ TeV and constraints on anomalous quartic gauge couplings*, J. High Energy Phys. **06**, 106 (2017), doi:10.1007/JHEP06(2017)106 [preprint doi:10.48550/arXiv.1612.09256].

[65] A. M. Sirunyan et al., *Measurement of vector boson scattering and constraints on anomalous quartic couplings from events with four leptons and two jets in proton-proton collisions at $\sqrt{s} = 13$ TeV*, Phys. Lett. B **774**, 682 (2017), doi:10.1016/j.physletb.2017.10.020 [preprint doi:10.48550/arXiv.1708.02812].

[66] A. M. Sirunyan et al., *Measurement of differential cross sections for Z boson pair production in association with jets at $\sqrt{s} = 8$ and 13 TeV*, Phys. Lett. B **789**, 19 (2019), doi:10.1016/j.physletb.2018.11.007 [preprint doi:10.48550/arXiv.1806.11073].

[67] M. Aaboud et al., *Observation of electroweak $W^\pm Z$ boson pair production in association with two jets in pp collisions at $\sqrt{s} = 13$ TeV with the ATLAS detector*, Phys. Lett. B **793**, 469 (2019), doi:10.1016/j.physletb.2019.05.012 [preprint doi:10.48550/arXiv.1812.09740].

[68] A. M. Sirunyan et al., *Measurement of electroweak WZ boson production and search for new physics in WZ + two jets events in pp collisions at $\sqrt{s} = 13$ TeV*, Phys. Lett. B **795**, 281 (2019), doi:10.1016/j.physletb.2019.05.042 [preprint doi:10.48550/arXiv.1901.04060].

[69] CMS collaboration: V. Khachatryan et al., *Evidence for exclusive $\gamma\gamma \to W^+W^-$ production and constraints on anomalous quartic gauge couplings in pp collisions at $\sqrt{s} = 7$ and 8 TeV*, J. High Energy Phys. **08**, 119 (2016), doi:10.1007/JHEP08(2016)119 [preprint doi:10.48550/arXiv.1604.04464].

[70] CMS collaboration: A. M. Sirunyan et al., *Observation of electroweak production of same-sign W boson pairs in the two jet and two same-sign lepton final state in proton-proton collisions at $\sqrt{s} = 13$ TeV*, Phys. Rev. Lett. **120**, 081801 (2018), doi:10.1103/PhysRevLett.120.081801 [preprint doi:10.48550/arXiv.1709.05822].

[71] A. M. Sirunyan et al., *Search for anomalous electroweak production of vector boson pairs in association with two jets in proton-proton collisions at 13 TeV*, Phys. Lett. B **798**, 134985 (2019), doi:10.1016/j.physletb.2019.134985 [preprint doi:10.48550/arXiv.1905.07445].

[72] A. M. Sirunyan et al., *Observation of electroweak production of $W\gamma$ with two jets in proton-proton collisions at $\sqrt{s} = 13$ TeV*, Phys. Lett. B **811**, 135988 (2020), doi:10.1016/j.physletb.2020.135988 [preprint doi:10.48550/arXiv.2008.10521].

[73] A. M. Sirunyan et al., *Evidence for electroweak production of four charged leptons and two jets in proton-proton collisions at $\sqrt{s} = 13$ TeV*, Phys. Lett. B **812**, 135992 (2021), doi:10.1016/j.physletb.2020.135992 [preprint doi:10.48550/arXiv.2008.07013].

[74] CMS collaboration, *Measurement of the electroweak production of $W\gamma$ in association with two jets in proton-proton collisions at $\sqrt{s} = 13$ TeV*, Phys. Rev. D **108**, 032017 (2023), doi:10.1103/PhysRevD.108.032017 [preprint doi:10.48550/arXiv.2212.12592].

[75] O. J. P. Éboli, M. C. Gonzalez-Garcia and J. K. Mizukoshi, $pp \to jje^\pm\mu^\pm\nu\nu$ and $jje^\pm\mu^\mp\nu\nu$ at $\mathcal{O}(\alpha_{em}^6)$ and $\mathcal{O}(\alpha_{em}^4\alpha_s^2)$ for the study of the quartic electroweak gauge boson vertex at CERN LHC, Phys. Rev. D **74**, 073005 (2006), doi:10.1103/PhysRevD.74.073005 [preprint doi:10.48550/arXiv.hep-ph/0606118].

[76] O. J. P. Éboli and M. C. Gonzalez-Garcia, *Classifying the bosonic quartic couplings*, Phys. Rev. D **93**, 093013 (2016), doi:10.1103/PhysRevD.93.093013 [preprint doi:10.48550/arXiv.1604.03555].

[77] M. Jacob and G. C. Wick, *On the general theory of collisions for particles with spin*, Ann. Phys. **281**, 774 (2000), doi:10.1006/aphy.2000.6022.

[78] C.-X. Yue, X.-J. Cheng and J.-C. Yang, *Charged-current non-standard neutrino interactions at the LHC and HL-LHC*, Chin. Phys. C **47**, 043111 (2023), doi:10.1088/1674-1137/acb993 [preprint doi:10.48550/arXiv.2110.01204].

[79] G. J. Gounaris, J. Laysaac and F. M. Renard, *Unitarity constraints for transverse gauge bosons at LEP and supercolliders*, Phys. Lett. B **332**, 146 (1994), doi:10.1016/0370-2693(94)90872-9 [preprint doi:10.48550/arXiv.hep-ph/9311370].

[80] T. Corbett, O. J. P. Éboli and M. C. Gonzalez-Garcia, *Unitarity constraints on dimension-six operators*, Phys. Rev. D **91**, 035014 (2015), doi:10.1103/PhysRevD.91.035014 [preprint doi:10.48550/arXiv.1411.5026].

[81] T. Corbett, O. J. P. Éboli and M. C. Gonzalez-Garcia, *Unitarity constraints on dimension-six operators. II. Including fermionic operators*, Phys. Rev. D **96**, 035006 (2017), doi:10.1103/PhysRevD.96.035006 [preprint doi:10.48550/arXiv.1705.09294].

[82] G. Perez, M. Sekulla and D. Zeppenfeld, *Anomalous quartic gauge couplings and unitarization for the vector boson scattering process* $pp \rightarrow W^+W^+jjX \rightarrow \ell^+\nu_\ell\ell^+\nu_\ell jjX$, Eur. Phys. J. C **78**, 759 (2018), doi:10.1140/epjc/s10052-018-6230-1 [preprint doi:10.48550/arXiv.1807.02707].

[83] E. da Silva Almeida, O. J. P. Éboli and M. C. Gonzalez-Garcia, *Unitarity constraints on anomalous quartic couplings*, Phys. Rev. D **101**, 113003 (2020), doi:10.1103/PhysRevD.101.113003 [preprint doi:10.48550/arXiv.2004.05174].

[84] W. Kilian, S. Sun, Q.-S. Yan, X. Zhao and Z. Zhao, *Multi-Higgs boson production and unitarity in vector-boson fusion at future hadron colliders*, Phys. Rev. D **101**, 076012 (2020), doi:10.1103/PhysRevD.101.076012 [preprint doi:10.48550/arXiv.1808.05534].

[85] W. Kilian, S. Sun, Q.-S. Yan, X. Zhao and Z. Zhao, *Highly boosted Higgs bosons and unitarity in vector-boson fusion at future hadron colliders*, J. High Energy Phys. **05**, 198 (2021), doi:10.1007/JHEP05(2021)198 [preprint doi:10.48550/arXiv.2101.12537].

[86] P. T. Komiske, E. M. Metodiev and J. Thaler, *Metric space of collider events*, Phys. Rev. Lett. **123**, 041801 (2019), doi:10.1103/PhysRevLett.123.041801 [preprint doi:10.48550/arXiv.1902.02346].

[87] CMS collaboration: A. M. Sirunyan et al., *Observation of electroweak production of Wγ with two jets in proton-proton collisions at* $\sqrt{s} = 13$ TeV, Phys. Lett. B **811**, 135988 (2020), doi:10.1016/j.physletb.2020.135988.

[88] J. Alwall et al., *The automated computation of tree-level and next-to-leading order differential cross sections, and their matching to parton shower simulations*, J. High Energy Phys. **07**, 079 (2014), doi:10.1007/JHEP07(2014)079 [preprint doi:10.48550/arXiv.1405.0301].

[89] N. D. Christensen and C. Duhr, *FeynRules – Feynman rules made easy*, Comput. Phys. Commun. **180**, 1614 (2009), doi:10.1016/j.cpc.2009.02.018 [preprint doi:10.48550/arXiv.0806.4194].

[90] C. Degrande, C. Duhr, B. Fuks, D. Grellscheid, O. Mattelaer and T. Reiter, *UFO – The universal FeynRules output*, Comput. Phys. Commun. **183**, 1201 (2012), doi:10.1016/j.cpc.2012.01.022 [preprint doi:10.48550/arXiv.1108.2040].

[91] J. de Favereau, C. Delaere, P. Demin, A. Giammanco, V. Lemaître, A. Mertens and M. Selvaggi, *DELPHES 3: A modular framework for fast simulation of a generic collider experiment*, J. High Energy Phys. **02**, 057 (2014), doi:10.1007/JHEP02(2014)057 [preprint doi:10.48550/arXiv.1307.6346].

[92] Y.-C. Guo, F. Feng, A. Di, S.-Q. Lu and J.-C. Yang, *MLAnalysis: An open-source program for high energy physics analyses*, Comput. Phys. Commun. **294**, 108957 (2024), doi:10.1016/j.cpc.2023.108957 [preprint doi:10.48550/arXiv.2305.00964].

[93] F. Pedregosa et al., *Scikit-learn: Machine learning in Python*, J. Mach. Learn. Res. **12**, 2825 (2011).

[94] D. Donoho and J. Jin, *Higher criticism for detecting sparse heterogeneous mixtures*, Ann. Stat. **32**, 962 (2004), doi:10.1214/009053604000000265 [preprint doi:10.48550/arXiv.math/0410072].

[95] G. Cowan, K. Cranmer, E. Gross and O. Vitells, *Asymptotic formulae for likelihood-based tests of new physics*, Eur. Phys. J. C **71**, 1554 (2011), doi:10.1140/epjc/s10052-011-1554-0 [preprint doi:10.48550/arXiv.1007.1727].

[96] P. A. Zyla et al., *Review of particle physics*, Prog. Theor. Exp. Phys. 083C01 (2020), doi:10.1093/ptep/ptaa104.

[97] K. M. Black et al., *Muon collider forum report*, J. Instrum. **19**, T02015 (2024), doi:10.1088/1748-0221/19/02/T02015 [preprint doi:10.48550/arXiv.2209.01318].

[98] C. Accettura et al., *Towards a muon collider*, Eur. Phys. J. C **83**, 864 (2023), doi:10.1140/epjc/s10052-023-11889-x [preprint doi:10.48550/arXiv.2303.08533].

[99] L. Jiang, Y.-C. Guo and J.-C. Yang, *Detecting anomalous quartic gauge couplings using the isolation forest machine learning algorithm*, Phys. Rev. D **104**, 035021 (2021), doi:10.1103/PhysRevD.104.035021 [preprint doi:10.48550/arXiv.2103.03151].